2003

A simple quantum mechanical treatment of scattering in nanoscale transistors

Rajesh Venugopal
Purdue University

Magnus Paulsson
Purdue University

Sebastien Goasguen
Purdue University, Main Campus

Supriyo Datta
Birck Nanotechnology Center and Purdue University, datta@purdue.edu

Mark S. Lundstrom
Purdue University, lundstro@purdue.edu

A simple quantum mechanical treatment of scattering in nanoscale transistors

R. Venugopal,[a] M. Paulsson, S. Goasguen, S. Datta, and M. S. Lundstrom
School of Electrical and Computer Engineering, Purdue University, 1285 Electrical Engineering Building, West Lafayette, Indiana 47907-1285

(Received 29 October 2002; accepted 31 January 2003)

We present a computationally efficient, two-dimensional quantum mechanical simulation scheme for modeling dissipative electron transport in thin body, fully depleted, *n*-channel, silicon-on-insulator transistors. The simulation scheme, which solves the nonequilibrium Green's function equations self consistently with Poisson's equation, treats the effect of scattering using a simple approximation inspired by the ''Büttiker probes,'' often used in mesoscopic physics. It is based on an expansion of the active device Hamiltonian in decoupled mode space. Simulation results are used to highlight quantum effects, discuss the physics of scattering and to relate the quantum mechanical quantities used in our model to experimentally measured low field mobilities. Additionally, quantum boundary conditions are rigorously derived and the effects of strong off-equilibrium transport are examined. This paper shows that our approximate treatment of scattering, is an efficient and useful simulation method for modeling electron transport in nanoscale, silicon-on-insulator transistors. © *2003 American Institute of Physics.* [DOI: 10.1063/1.1563298]

I. INTRODUCTION

Metal oxide field effect transistors (MOSFETs) with channel lengths in the 10 nm regime have been recently demonstrated by several research groups.[1,2] Design considerations to yield devices with desirable channel lengths have been theoretically explored in Refs. 3–5. The smallest devices use a silicon-on-insulator (SOI) geometry in which electron transport occurs in a thin silicon film which is sandwiched between two insulators. Device physics in such structures has been examined mainly in the pure ballistic limit and in some cases by invoking simple one-dimensional (1D) approximations. Real devices typically operate below the ballistic limit as a result of scattering. Therefore, our primary objective in this article is to describe a computationally efficient, quantum mechanical treatment of scattering in *n*-channel MOSFETs based on the nonequilibrium Green's function formalism.[6,7]

Scattering within a device can be due to several reasons. Microscopically, electrons are confined within a very narrow channel and the channel is sandwiched between insulators in SOI devices. These insulator surfaces are never perfectly smooth, and the semiconductor lattice is never defect free. Therefore electrons in the channel experience surface roughness scattering. Both, channel carrier densities and impurity concentrations are typically very large. Therefore there is significant electron-electron and electron-impurity scattering within the device. Moreover, devices typically operate at relatively high temperatures (greater than 300 K) resulting in strong phonon–electron interactions. All these mechanisms need to be considered for an accurate treatment of scattering. Currently, solutions to the Boltzmann equation using Monte Carlo methods offer the best platform for modeling the effects of scattering in detail. Although comprehensive in their treatment of scattering, these simulation platforms do not treat quantum effects rigorously. As critical device dimensions are shrunk, quantum effects begin to manifest themselves strongly. These effects need careful consideration because they affect critical device performance metrics. However, a simulation platform based on quantum mechanics, which also treats the effects of each scattering mechanism individually is not computationally viable. Therefore an approximate treatment of scattering, which in addition captures the effect of source-to-channel tunneling and includes quantum effects which affect the threshold voltage and gate capacitance is clearly useful for device design.

Within the nonequilibrium Green's function (NEGF) formalism, a detailed treatment of the various scattering processes (e.g., surface roughness, phonon, impurity etc.) is possible. However, due to the large computational cost involved in a detailed simulation of a MOSFET, scattering is treated approximately using the concept of Büttiker probes. Although introduced phenomenologically by Büttiker,[8,9] a comparison with the detailed NEGF scattering treatment provides insights and allows us some control over the approximation. Büttiker probes are used to simulate the effect of scattering due to all possible mechanisms and including the effect of degeneracy. Our scattering model is a one parameter fitting model and the parameter that we use is analytically related to an equivalent mobility (Appendix B). From a design perspective, it is important to be able to calibrate the parameters used in our quantum mechanical model to mimic an equivalent low field mobility because the low field mobility can be measured experimentally. Such a calibration enables us to relate our results to those obtained from conventional simulation tools, thus serving as a benchmark which can be used to validate simpler models (based on the density gradient and

[a]Author to whom correspondence should be addressed; electronic mail: venugopr@ecn.purdue.edu

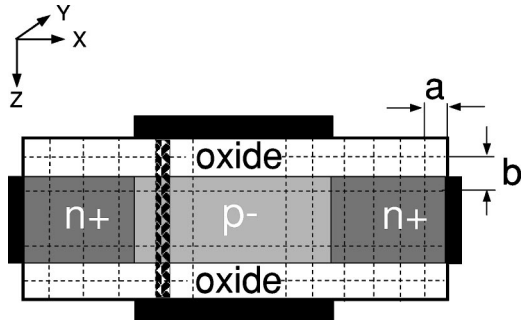

FIG. 1. An ultrathin body DG MOSFET structure with S/D doping of $10^{20}\,\mathrm{cm}^{-3}$ and an intrinsic channel (channel thickness=1.5 nm). A slice of the device within which a 1D, *z* directed effective mass equation is solved, is also indicated.

effective potential treatments).[10,11] It also helps fit our parameters to measured device data in a meaningful fashion.

Irrespective of the technique used to simulate scattering, the essential physics of scattering has to be captured.[12] This physics can be summarized by considering the on-state of a MOSFET with electrons thermally injected from the source, undergoing scattering in the channel and being collected by the drain. Scattering can occur anywhere inside the device, but for a fixed potential profile, only those scattering events occurring in the low field region near the source have the largest effect on the on-current. Although the scattering rate in the high field region near the drain can be very large, electrons scattering near the drain end are forced by the high electric fields to leave the channel, having little chance making it back to the source. Therefore scattering in this region does not degrade the on-state current directly (although it does do so indirectly through its effect on the self-consistent potential profile). We demonstrate that our transport model does capture this essential physics of scattering.

This article describes the numerical methods used to treat the effects of dissipative transport with specific emphasis on relating Büttiker probe strengths to low field mobilities and on the essential physics of scattering. Quantum boundary conditions are derived and quantum mechanical features of the simulation results are highlighted. The article is divided into the following sections: Sec. II presents the solution scheme. Section III presents simulation results obtained by applying the scattering model to a nanoscale, double-gate (DG), *n*-channel MOSFET. Section IV compares two different versions of the scattering model with regards to the essential physics and Sec. V summarizes key findings.

II. THEORY

The simulated device structure is shown in Fig. 1. A uniform rectangular grid with a grid spacing of *a*, along the *x* direction and *b* along the *z* direction is used. Note that we restrict our focus to the intrinsic device and account for the large source/drain (S/D) reservoirs to which the device is coupled, using open boundary conditions (no *x* dependence of the potential). The Fermi levels at the ends of the intrinsic device are specified by the applied voltage. The width (*y* dimension) of the device is assumed to be large and all potentials (including the scattering potential) are assumed to be translationally invariant along the width (*W*). A single band effective mass Hamiltonian is used to model carrier transport. In our modeling scheme, the scattering potential is treated as a perturbation to the ballistic device Hamiltonian. Therefore we briefly review the steps common to both ballistic and dissipative transport models.

A. The ballistic solution

We begin by solving a 1D, *z* directed effective mass equation for each vertical slice along *x* (Fig. 1), to obtain a set of eigenenergies and eigenfunctions (modes) along the gate confinement direction. The equation that is solved is

$$-\frac{\hbar^2}{2m_z^*}\frac{\partial^2}{\partial^2 z}\Psi_i(x,z)-qV(x,z)\Psi_i(x,z)=E_i(x)\Psi_i(x,z) \tag{1}$$

where m_z^* is the electron effective mass in the *z* direction, $V(x,z)$ the electrostatic potential, *q* the electron charge, and $\Psi_i(x,z)$ and $E_i(x)$, the wave function and eigenenergy for mode *i* at slice *x*, respectively. Note that the simulation domain in the confinement direction can be extended to include the insulator regions. Each vertical slice has a width *a* and within each slice, all quantities are assumed to be a constant in the *x* direction.

We then expand the three-dimensional (3D) effective mass Hamiltonian for the device in terms of $\delta(x-x')\Psi_i(x,z)$ and $e^{jk_jy}/\sqrt{W}$. The plane wave function, $e^{jk_jy}/\sqrt{W}$, represents the device width and the quantum number k_j, corresponds to the eigenenergy, $E_{k_j}=\hbar^2k_j^2/2m_y^*$, where m_y^* is the electron effective mass in the *y* direction. We use plane waves to represent the device width because all potentials are assumed to be invariant along *y*. The over all wavefunction in this orthonormal basis is

$$\Phi(x',y,z)=\sum_{i=1}^{\infty}\tilde{\Phi}_i(x')\Psi_i(x',z)e^{jk_jy/\sqrt{W}}, \tag{2}$$

where $\tilde{\Phi}_i(x')$, is the expansion coefficient of $\Psi_i(x',z)$ and the summation over *i* runs over all the modes. If we assume that the shape of a mode does not change as we move from the source to the drain $(\partial\Psi_i(x,z)/\partial x=0)$ and invoke the orthogonality criterion $[\int\Psi_i^*(x,z)\Psi_j(x,z)dz=\delta_{ij}]$, the 3D effective mass Hamiltonian reduces to a set of decoupled 1D Hamiltonians (one for each mode *i* and k_j) of the form

$$-\frac{\hbar^2}{2m_x^*}\frac{\partial^2\tilde{\Phi}_i(x')}{\partial^2x'}+E_i(x')\tilde{\Phi}_i(x')=[E-E_{k_j}]\tilde{\Phi}_i(x'), \tag{3}$$

where *E* is the total electron energy and $E_L=E-E_{k_j}$ is the longitudinal or channel directed electron energy. Equation (3) is the decoupled mode-space transformation of the 3D effective mass Hamiltonian. It is the starting point for simulating both ballistic and dissipative transport in thin body, fully depleted, SOI transistors. A detailed expansion of the 3D Hamiltonian and the validity of the decoupled mode-space solution has been presented in Ref. 13. Simplified versions of the decoupled mode-space solution scheme have been extensively used by several authors to model electron

transport in both SOI and carbon nanotube transistors in the literature.[3,5,14] The decoupled mode-space solution is a computationally efficient method to model electron transport in ultrathin SOI transistors because only a few low energy modes are occupied in these devices even at room temperature. High energy modes which are unoccupied, can be safely ignored without any loss of accuracy. Note that the 1D Hamiltonian is coupled to the electrostatic potential through the Poisson equation. The mode-space solution is therefore obtained self consistently. The NEGF formalism is not only an effective method to simulate the ballistic MOSFET, but also allows for scattering to be included either in detail or approximately.

B. The scattering model

In the ballistic limit, there are only two reservoirs connected to a device, namely, the source and drain contacts. These contacts inject carriers into and extract carriers from the intrinsic device while conserving the current (net current at the source contact equals the net current at the drain contact). In the presence of scattering, Büttiker probes can be used to model dissipative transport phenomenologically within the transistor.[8,15] These Büttiker probes perturb the Hamiltonian of the device in a manner similar to the source and drain contacts and can also be viewed as reservoirs coupled to the device. However, the fundamental difference between the real S/D reservoirs and those represented by Büttiker probes is that the probes can only change the electron energy/momentum and not the electron number within the device. This implies that one can view a Büttiker probe as extracting electrons from the device, perturbing the energy/momentum of those electrons and reinjecting an equal number back into the system with a different energy/momentum distribution. The coupling energy between the device and the probes can be adjusted to vary the scattering strength smoothly from zero (ballistic transport) to a high value (diffusive transport) as illustrated in Appendix A.

The Fermi energy characterizes how a reservoir exchanges carriers with the device. Since Büttiker probes extract and inject electrons into the system, they have an associated Fermi energy that should be adjusted to achieve carrier conservation within the device. Carrier conservation at each scattering center (zero probe current) guarantees current continuity through the transistor even in the presence of scattering.

To include the effects of dissipative transport, we start with the 1D Hamiltonian [Eq. (3)] in the transmission direction (x) for mode i. This Hamiltonian is discretized on a finite difference grid to obtain a tridiagonal matrix of the form

$$h_i=\begin{bmatrix} \ddots & \ddots & \ddots & \cdots & \cdots \\ -t_{x,i} & 2t_{x,i}+E_i(1) & -t_{x,i} & 0 & \cdots \\ 0 & \ddots & \ddots & \ddots & 0 \\ \cdots & \ddots & -t_{x,i} & 2t_{x,i}+E_i(N_X) & -t_{x,i} \\ \cdots & \ddots & \ddots & \ddots & \ddots \end{bmatrix} \tag{4}$$

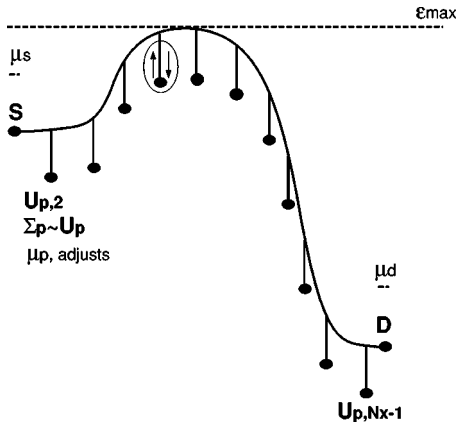

FIG. 2. The profile of a generic mode is illustrated along with the placement of Büttiker probes. Note that the Fermi level of the S/D contacts is fixed, while that of the probe is adjusted to preserve the number of carriers. The probe self energy is related to the coupling strength.

where N_X is the number of grid points and t_x, the coupling energy between adjacent grid points along the channel. The coupling energy is

$$t_{x,i}=\frac{\hbar^2}{2m^*_{x,i}a^2}, \tag{5}$$

where a is the grid spacing and $m^*_{x,i}$, the electron effective mass in the x direction for mode i. We attach semi-infinite, 1D, Büttiker probes to each mode i, as shown in Fig. 2. Two unknowns, namely the bandwidth and the band center, define the density of states within a probe. These parameters cannot be chosen arbitrarily since they affect the Büttiker probe approximation. However, a comparison with the detailed NEGF scattering formalism ensures that the approximation gives physically reasonable results when the density of states within the probes coincides with that of the device. This is discussed further in Sec. III. Each probe is characterized by a coupling energy U_p and by a Fermi level μ_p (Fig. 2). The quantity that we are interested in is the retarded Green's function for mode i within the intrinsic device region [the corresponding Hamiltonian is the matrix within the box in Eq. (4)]. The Green's function, at a specific longitudinal energy ($E_L=E-E_{k_j}$), is

$$G_i[E_L]=[E_LI-h_i-\Sigma_i(E_L)]^{-1}. \tag{6}$$

Note that Eq. (4) represents an infinite 1D Hamiltonian (because the S/D contacts are infinite). However, all of the effects associated with coupling a finite device to infinite S/D reservoirs and the effect of scattering within the device can be accounted for by introducing an appropriate self-energy matrix, which is denoted by $\Sigma_i(E_L)$ (refer to Appendix A for details of the self-energy calculation). The self-energy concept allows us eliminate the semi-infinite reservoirs and work solely within the device subspace whose dimensions are much smaller. It is

$$\Sigma_i[E_L]=\begin{bmatrix} -t_x e^{jk_{x,1}a} & 0 & 0 & \cdots \\ 0 & -\dfrac{|U_2|^2}{t_x}e^{jk_{x,2}a} & 0 & \cdots \\ \ddots & \ddots & \ddots & \ddots \\ \ddots & \ddots & -\dfrac{|U_{N_X-1}|^2}{t_x}e^{jk_{x,N_X-1}a} & \ddots \\ \ddots & \ddots & \ddots & -t_x e^{jk_{x,N_X}a} \end{bmatrix}, \tag{7}$$

where $j=\sqrt{(-1)}$. On including the self-energy matrix [Eq. (7)], the size of the discrete Green's function matrix for mode i is N_X^2. Since Büttiker probes represent isolated scattering centers, the self-energy matrix is diagonal and has nonzero entries only at those points where a probe has been introduced. Note that the self energy for a probe is proportional to U_p [Eq. (7)]. Just as t_x represents the coupling strength between adjacent points within the device, U_p represents the coupling strength between points in the device and points in the probe. If this energy is large, it implies that an electron in the device can easily scatter into the probe. When U_p tends to zero, there is no coupling between the device and the probes and electrons ballistically traverse the intrinsic device region. An analytic relation between the probe coupling energy and the mean free path is presented in Appendix B. It should be noted that although we use 1D probes, the nature of the probes can be easily modified by adjusting the probe self-energy. This may provide a useful technique for mimicing scattering processes in other systems.

Once the retarded Green's function is evaluated, electron density and current due to injection from the S/D contacts and all of the Büttiker probes can be easily computed. We define a new quantity in terms of the self-energy as $\Gamma_i = j(\Sigma_i - \Sigma_i^\dagger)$.[9,7] This broadening function describes the electron exchange rate between the active device and all of the reservoirs to which the device is coupled. The state spectral functions due to injection from the S/D and all probes for mode i is

$$A_i^n[E_L]=G_i[E_L]\Gamma_i^n[E_L]G_i^\dagger[E_L], \tag{8}$$

where n runs over all the reservoirs (including the S/D). Note that A_i^n is a matrix with the same size as G_i, and that its diagonal entries constitute the local density of states (LDOS) due to injection from reservoir n

$$D_i[E_L,m]=\frac{1}{2\pi}(A_i^n[E_L])^{mm}=\frac{1}{2\pi}|G_i^{mn}|^2\Gamma_i^n. \tag{9}$$

Conceptually, the spectral function is proportional to perturbation strength Γ_i^n and propagates through the entire domain according to $|G_i^{mn}|^2$. Since G_i^{mn} (with a running index m) is the nth column of G, one does not need to calculate the entire G (computationally expensive) in order to obtain the spectral function. Only those columns corresponding to S/D contacts or Büttiker probe positions need to be calculated. Thus it is clear that in the ballistic case, we need only the first and last columns of G, while with scattering turned on everywhere, the entire G needs to be evaluated. Transmission between any two reservoirs labeled m and n is

$$T_i^{mn}[E_L]=\mathrm{Trace}[\Gamma_i^m G_i \Gamma_i^n G_i^\dagger]=\Gamma_i^m|G_i^{mn}|^2\Gamma_i^n. \tag{10}$$

Knowing the LDOS [Eq. (9)], the two-dimensional (2D) electron density at node m, for mode i, including the effect of all scattering centers and the S/D is

$$n_i[E_L,m]=\frac{1}{\pi a}\sum_n \int_0^\infty \sqrt{\frac{m_{y,i}^*}{2\hbar^2 E_{k_j}}}(A_i^n)^{mm}[E_L] \times f[\mu_n, E_L+E_{k_j}]dE_{k_j}, \tag{11}$$

where n is the reservoir index that runs over all the probes and the S/D, f the Fermi–Dirac function for reservoir n and $\sqrt{m_{y,i}^*/2\hbar^2 E_{k_j}}$ the transverse mode state density for subband i (including spin degeneracy). Since the spectral function, $(A_i^n)^{mm}$ depends on the longitudinal energy alone [Eq. (8)], it can be moved out of the integral in Eq. (11) which reduces to

$$n_i[E_L,m]=\frac{1}{\hbar a}\sqrt{\frac{m_{y,i}^* k_B T}{2\pi^3}}\sum_n (A_i^n)^{mm}[E_L] \times F_{-1/2}[\mu_n - E_L], \tag{12}$$

where the argument of the $F_{-1/2}$ function has been normalized by $k_B T$ (for an analytic form of $F_{-1/2}$, refer to Ref. 16). The net 2D electron density at node m is obtained by summing contributions from all modes and valleys. In a similar fashion, the net current at reservoir m including contributions from all reservoirs (n), modes (labeled by i) and valleys is

$$I^m[E_L]=\frac{q}{\hbar^2}\sum_i \sqrt{\frac{2m_{y,i}^* k_B T}{\pi^3}}\sum_n T_i^{mn}[F_{-1/2}(\mu_m - E_L) - F_{-1/2}(\mu_n - E_L)]. \tag{13}$$

Note that the index n includes the S/D contacts as well and that the transmission between nodes m and n is as specified by Eq. (10). Also note that while the Fermi level of the S/D contacts is fixed by the applied voltage, the Fermi level of the Büttiker probes has to be determined from current continuity. Current continuity requires that the net current at each probe equals zero. This implies that

$$I^m=\int_{-\infty}^{\infty} I^m[E_L]dE_L=0$$

or

$$I^m[E_L]=0 \tag{14}$$

for each E_L at each probe (probe indices are denoted by m).[17] Equation (14) imposes a set of constraints on the Fermi potentials of the probes. These constraining equations are solved for the probe Fermi levels.

Note that Eq. (14) provides two options to ensure that the net current at each scattering center equals zero. Both of these options are examined in this paper as they represent different phenomenological treatments of scattering. In the first model, we assume that the net current at each scatterer, when integrated over all E_L equals zero i.e., $\int_{-\infty}^{\infty} I^m[E_L]dE_L=0$. This requirement implies that electrons from all modes are fully thermalized at each probe according to the corresponding probe Fermi potential and temperature (the local distribution is Fermi–Dirac). It also implies that the probe Fermi potentials are just position and not energy dependent. We will refer to this treatment of scattering as the energy relaxed probe model because the longitudinal energy of the electrons within the device is relaxed due to scattering. In the second model we assume that the current at each scatterer equals zero for each E_L. Therefore, Eq. (14) is trivially satisfied. However, in this model, the Fermi level of the Büttiker probes are both position and longitudinal energy dependent because we obtain a set of chemical potentials for the probes at each E_L (Note that although we refer to the chemical potential of the probe as a Fermi potential for mathematical convenience, the distribution locally is not Fermi–Dirac). We will refer to this model as the phase breaking scattering model because the channel directed energy of the electrons is not relaxed although the channel directed momentum is relaxed. Irrespective of our choice of the scattering model, it should be noted that carrier populations in different modes are mixed as a result of scattering because the net current at a probe includes a sum over all modes. Therefore both models capture the effect of intervalley scattering.

In case of the energy relaxed model, the position dependent probe potentials can be adjusted iteratively using Newton's method because the constraining equations are nonlinear (due to the integration over E_L). The Jacobian matrix for the Newton iteration scheme is numerically evaluated as [Eqs. (10) and (13)]

$$\begin{aligned} J^{mm}&=\frac{\partial I^m}{\partial \mu_m}=\frac{q}{\hbar^2}\int_{-\infty}^{\infty}\sum_i \sqrt{\frac{2m^*_{y,i}k_BT}{\pi^3}} \\ &\quad\times\left\{\frac{\partial F_{-1/2}(\mu_m-E_L)}{\partial \mu_m}\sum_n T_i^{mn}\right\}dE_L, \\ J^{mn}&=\frac{\partial I^m}{\partial \mu_n}=-\frac{q}{\hbar^2}\int_{-\infty}^{\infty}\sum_i \sqrt{\frac{2m^*_{y,i}k_BT}{\pi^3}} \\ &\quad\times\left\{T_i^{mn}\frac{\partial F_{-1/2}(\mu_n-E_L)}{\partial \mu_n}\right\}dE_L \end{aligned} \tag{15}$$

and the corrections to the probe potentials during the solution searching iterations as

$$\Delta\mu^{\text{probes}}=-J^{-1}I^{\text{probes}}. \tag{16}$$

Note that the S/D Fermi levels are specified by the applied voltage, therefore the size of the Jacobian in Eq. (15) is $(N_X-2)^2$ although the summation index n in Eq. (15), includes the S/D contacts. For the phase-breaking model, we directly solve for the occupancy function $F_{-1/2}(\mu_m-E_L)$, at each longitudinal energy using a linear solution scheme of the form $AF_{-1/2}=B$ because there is no energy integral to be dealt with. Here, A and B, which are E_L dependent are

$$\begin{aligned} A^{mm}&=\frac{q}{\hbar^2}\sum_i \sqrt{\frac{2m^*_{y,i}k_BT}{\pi^3}}\sum_{n\neq m} T_i^{mn}, \\ A^{mn}&=-\frac{q}{\hbar^2}\sum_i \sqrt{\frac{2m^*_{y,i}k_BT}{\pi^3}}T_i^{mn}, \\ B^m&=[T^{m1}F_{-1/2}(\mu_s-E_L)+T^{mN_X}F_{-1/2}(\mu_d-E_L)]. \end{aligned} \tag{17}$$

In Eq. (17), the summation index n runs over all the reservoirs including the S/D contacts for the diagonal terms and over the probes alone for the off-diagonal terms of A, while index m runs over the probes alone (μ_s is the source Fermi level and μ_d the drain Fermi level). We mainly focus on the energy relaxing probe model in this article because this model seems to capture the essential physics of scattering more accurately within a nanoscale transistor when compared to the phase breaking model (Sec. IV).

Once the probe distribution functions have been evaluated using either Eqs. (15) and (16) or Eqs. (17), the net 2D charge density (n_i) for mode i can be calculated by integrating Eq. (11) over E_L. The 3D charge density at each node of our 2D real-space grid is obtained by multiplying n_i with the corresponding distribution function $|\Psi_i(x,z)|^2/b$, and by summing over all modes (i's) and conduction band valleys. Since the eigenvalue problem is solved exactly in the z direction (Fig. 1), quantum effects associated with confinement are accurately treated within our modeling scheme. This 3D density is used to solve Poisson's equation for a potential, and the self-consistent process repeated till convergence is achieved.

III. RESULTS

The simulated device structure (Fig. 1) is an ultrathin body, fully depleted, symmetric, dual gate n-MOSFET with the S/D regions doped at $10^{20}/\text{cm}^{-3}$ and an intrinsic channel. The gate length is 10 nm and there is no gate-to-S/D overlap. The S/D extensions are 10 nm and the junctions are abrupt. In order to highlight quantum effects and the effect of dissipative transport, we choose a thin silicon body (1.5 nm), which exhibits single mode occupancy. The oxide thickness (1 nm) and power supply voltage ($V_{\text{DD}}=0.4$ V) are set based on the International Technology Roadmap for Semiconductors (ITRS).[18] We adjust the gate work function for both the top and bottom gates to obtain a ballistic off-current of 10 μA/μm, consistent with the ITRS requirement. Gate oxides are treated as infinite potential barriers for electrons in all of our simulations. For scattering simulations, the input parameter is a position dependent low field mobility (Appendix B, provides an analytical relation between the mobility and

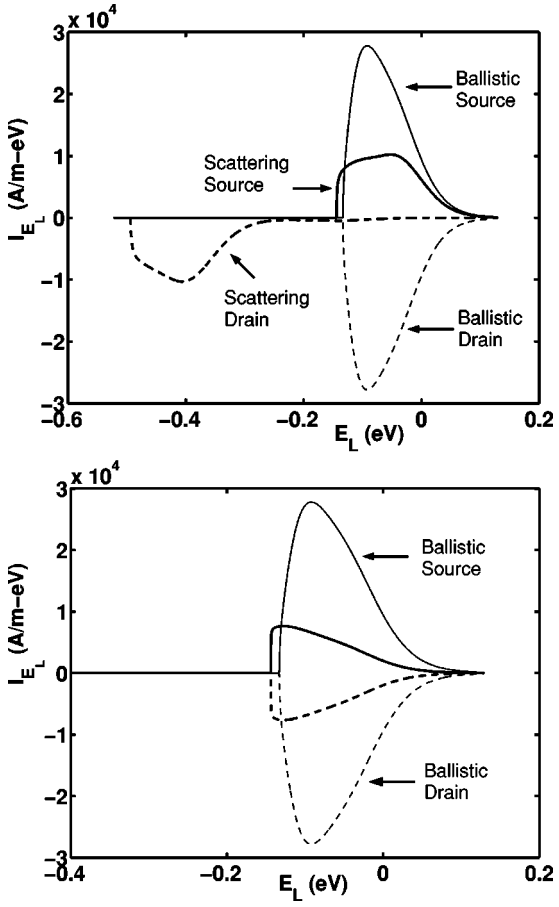

FIG. 3. (a) The current spectrum from the energy relaxed scattering model is compared against the ballistic limit in the on-state ($V_{GS}=V_{DS}=0.4$ V). Note that the drain current spectrum is relaxed in energy. (b) The current spectrum from the phase relaxed scattering model is compared against the ballistic limit, in the on state. The source and drain spectra are identical in the presence of scattering, because this model relaxes channel directed momentum only.

scattering strength). Measured low field mobilities of $\sim$200 $cm^2/V\,s$ (at a charge density of $\sim 10^{13}/cm^{-2}$) have been reported in the literature, for silicon film thicknesses of $\sim$5 nm.[19–21] As the silicon film thickness is reduced, there are two competing effects which affect the mobility. Increased surface roughness scattering reduces the low field mobility, while confining all of the electrons to the unprimed bands raises the low field mobility.[22] Therefore, as an approximation, we assume that these effects cancel, and that a low field mobility of 200 $cm^2/V\,s$ is a reasonable value to use in the channel region (our channel charge is also $\sim 10^{13}/cm^{-2}$ in the on state). For the S/D extensions which are highly doped, we use a doping dependent mobility model that yields a value of 55 $cm^2/V\,s$ at a donor doping concentration of $\sim 10^{20}/cm^{-3}$.

In order to highlight quantum effects and present a general picture of how the Büttiker probe models work, we compare internal quantities with and without scattering within our model device. Figure 3 shows the self-consistent current spectrum versus longitudinal energy [Eq. (13)] in the on state ($V_{GS}=V_{DS}=0.4$ V) from both, the energy-relaxing [Fig. 3(a)] and the phase-breaking scattering models [Fig. 3(b)]. The ballistic current is superposed on each of the figures for comparison. In the ballistic limit, electrons enter the device from the source and leave though the drain. Both, the number and the energy of the electrons are conserved throughout the device. This is clear from Fig. 3(a), which indicates that the ballistic current spectra (light lines) at the source and drain ends are symmetric (while reading this plot, it should be noted that source injected current is positive for electrons entering the device, while the drain collected current is negative for electrons leaving the device). If we compare this ballistic spectra to the one obtained from the energy relaxed Büttiker probe model, we observe that the source injected current is reduced in magnitude, and the drain collected current no longer mirrors the source current distribution. This is because this model strongly relaxes the channel directed energy of the electrons injected from the source. These electrons leave the device with lower longitudinal energies because they lose energy due to scattering. The phase breaking model, [Fig. 3(b)] on the other hand, preserves the longitudinal energy of electrons, thus resulting in a symmetric spectrum (similar to the ballistic case). It should be noted that although the current spectra are symmetric, the current magnitude is reduced when compared to the ballistic case, because back scattered electrons lose their directed momentum due to scattering. We will mainly focus on results obtained using the energy relaxing model for the rest of this section. A more detailed comparison between the energy and phase relaxing scattering models is deferred to Sec. IV of this article.

Figure 4 compares the LDOS [Eq. (9)] and the 2D charge density spectra [Eq. (11)] versus longitudinal energy, with and without scattering ($V_{GS}=V_{DS}=0.4$ V). Note that Fig. 4 is plotted for a qualitative comparison only and that white areas in the figure represent a high density. The first mode is superposed on each of the plots in Fig. 4 (dotted white line) to indicate the effective potential energy of electrons. In the ballistic case, there is no phase relaxation within the device. Therefore, states injected from the drain end of the device undergo reflections and interfere strongly to the right of the source-to-channel barrier. This interference results in coherent oscillations in the LDOS as seen in Fig. 4(a) (left). When scattering is turned on throughout the device, phase information of the electrons within the device is randomized and the energy levels are broadened when compared to the ballistic case. Therefore, all of the interference effects are washed out as seen in Fig. 4(a) (right). Note that both, the ballistic LDOS and the LDOS with scattering, exhibit nonzero values below the source-to-channel barrier resulting in source-to-channel tunneling. In the ballistic case, the charge density spectrum (the square root of the charge is plotted to resolve low charge densities at the drain end) can be resolved into two components; one due to source injection and the other due to drain injection. The source injected charge propagates from the source to the drain without any energy relaxation, resulting in a ballistic peak in the charge spectrum at the drain end, as seen in Fig. 4(b) (left). The drain injected charge on the other hand, is completely reflected by the source-to-channel barrier in the on state. When scattering is turned on, the longitudinal energy of the electrons is relaxed (in case of the energy relaxing model) and the source and drain populations can no longer be distin-

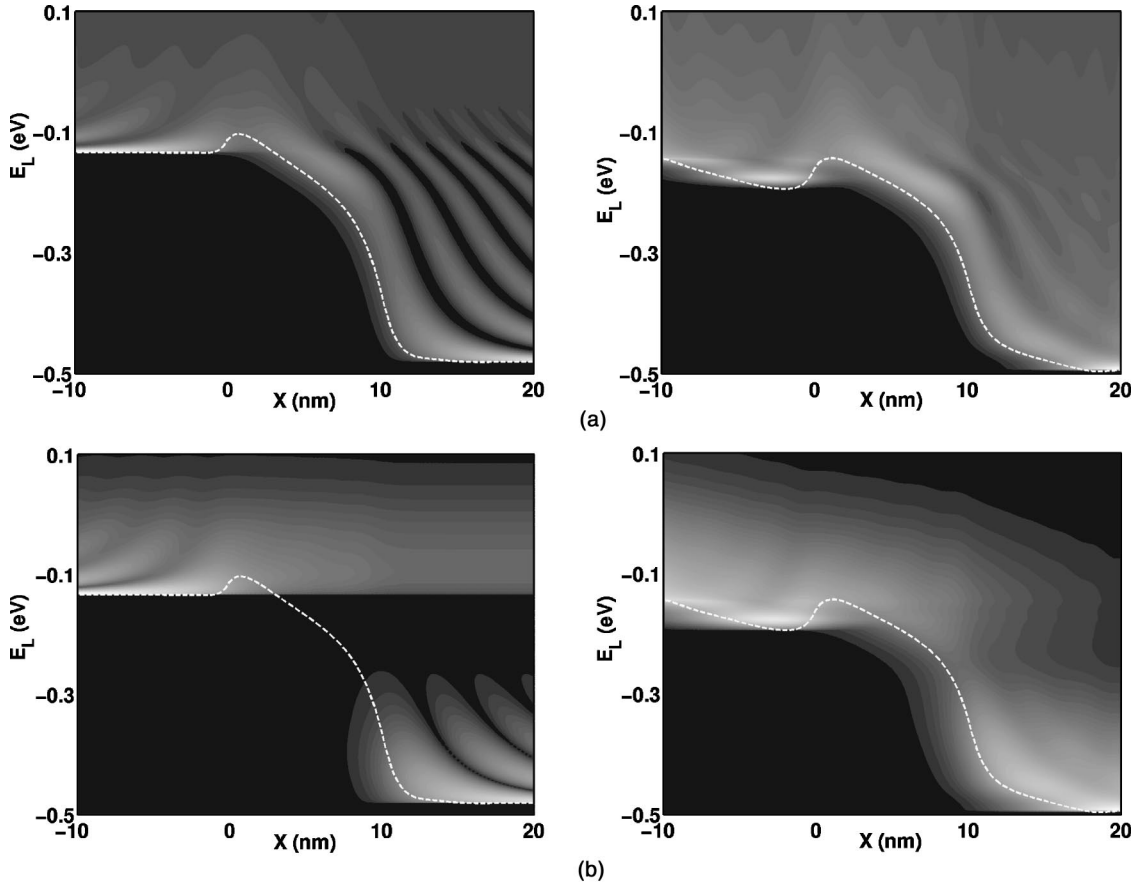

FIG. 4. (a) The local density of states in the on-state, from the ballistic (left) and energy relaxed scattering models (right). The first mode is also plotted (dotted line). Note that coherent oscillations in the LDOS are washed out when scattering is turned on. (b) The charge density spectrum from the ballistic (left) and energy relaxed scattering models (right), in the on state. In the ballistic limit, the source and drain injected populations can be clearly identified. When scattering is turned on, these populations are mixed.

guished. Also, any coherencies in the charge spectrum are also washed out as seen in Fig. 4(b) (right).

Next, we look at the full range I_{DS} versus V_{GS} characteristics for the model device with and without scattering in Fig. 5(a). Current in the off-state ($V_{GS}=0$, $V_{DS}=0.4\,V$), is comprised of two components; source-to-channel tunneling, for longitudinal energies below the source-to-channel barrier, and diffusion, for energies above the barrier. Scattering, in general, broadens the LDOS as discussed earlier. Therefore, the tunneling current component is increased in the off-state as a result of scattering, when compared to the ballistic limit. However, the detailed NEGF scattering model indicates that the scattering rate should be proportional to the LDOS at each energy.[9] Therefore, by choosing the energy band of the Büttiker probes to coincide with the local energy band within the device [Eq. (7)], we ensure that the broadening in the LDOS due to scattering and thus the increase in the tunneling current is not uncontrolled. This is particularly important when modeling low power devices where the off-current is dominated by tunneling.

The diffusion current component reduces when scattering is turned on, because the degenerate thermal injection velocity is reduced when compared to the ballistic limit.[23] Therefore, the cumulative effect of reduced diffusion and increased tunneling in the presence of scattering, is that the ballistic off current is always higher than the off current in the presence of scattering. This is clearly seen from Fig. 5(b), where we plot the off current versus channel length for channel lengths down to 5 nm. The ballistic off current sets an upper limit on the leakage current and provides a fairly accurate picture of the subthreshold behavior as transistors are scaled to smaller dimensions.

The Fermi level of each scatterer is adjusted to conserve current in the presence of scattering [Eqs. (15) and (16)]. This quantity, which is analogous to the quasi Fermi level computed in semiclassial models, has a clear physical interpretation. Unlike the quasi Fermi level (which is derived from the charge instead of the current), the Fermi level of the Büttiker probes is an actual representation of how the potential drops from the source to the drain. Figure 6(a), plots this quantity in the linear region ($V_{DS}=10\,mV$) of operation. In the off state, the channel resistance is high. Therefore all of the applied voltage drops in the channel region of the device. As the gate voltage increases, the channel conductivity increases, and the voltage dropped in the channel is reduced. This leads to a flattened Fermi potential profile in the channel and large voltage drops in the S/D regions. In the ballistic limit, there is no mechanism for internal voltage drop and all of the V_{DS} is dropped across the contact/device interface, resulting in a finite ballistic current. Note that the source

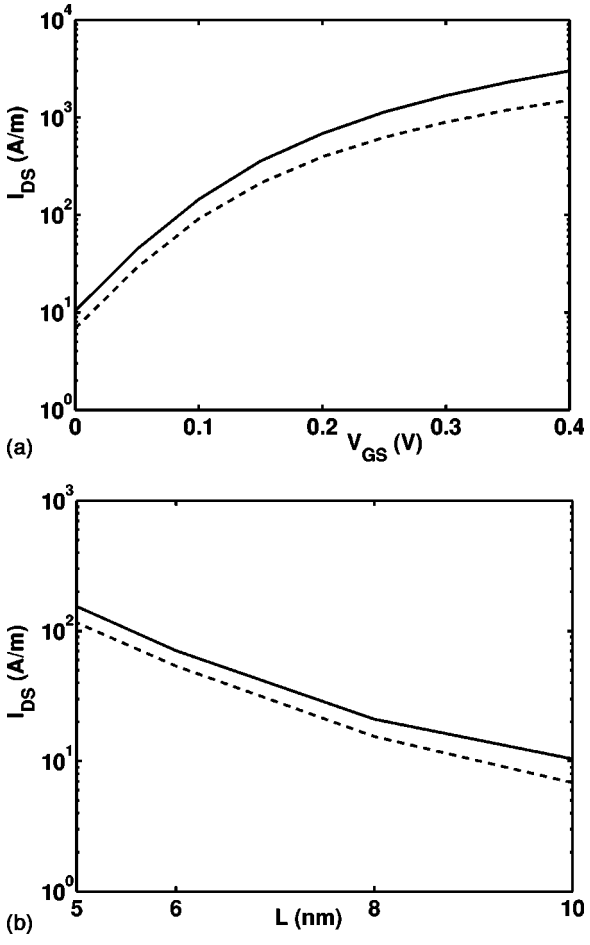

FIG. 5. (a) I_{DS} vs V_{GS} characteristics from the ballistic (solid line) and energy relaxed scattering models (dashed line) for $V_{DS}=0.4$ V. The off current, from the scattering model is lower despite an increase in the tunneling current due to a broadening in the LDOS below the source-to-channel barrier. (b) The off current vs channel length from the ballistic (solid line) and energy relaxed scattering models (dashed line). Ballistic simulations are good enough to evaluate leakage and subthreshold characteristics.

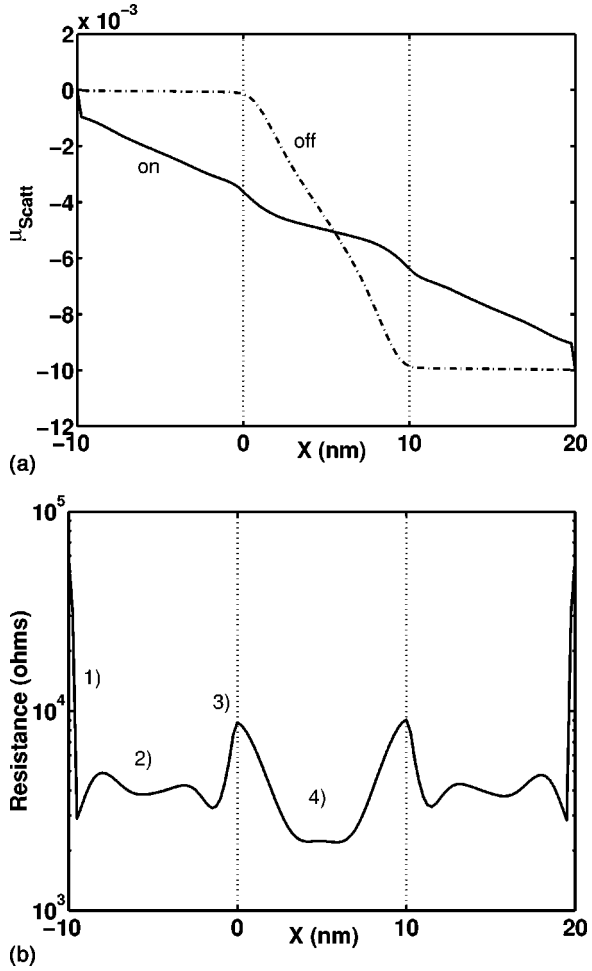

FIG. 6. (a) The self-consistent Fermi level of the Büttiker probes, from the energy relaxed scattering model, in the linear response region ($V_{DS}=10$ mV). (b) The extracted sheet resistivity in the on-state. Note the four components of the resistance: (1) quantum contact resistance, (2) S/D resistance, (3) tip resistance, and (4) channel resistance.

(drain) Fermi potential represents the Fermi energy of source (drain) injected carriers. In the off state there is very little current flow within the device and near equilibrium conditions prevail at both, the source/device and the drain/device interfaces. However, as the device is turned on, the distribution at the source/device interface (and the drain/device interface) is strongly off equilibrium in order to maintain a large current flow. This leads to the observed discontinuity in the Fermi potential at the contact/device interface as seen in Fig. 6(a).

In the linear region, it is possible to derive the sheet resistivity versus position along the channel, from the probe Fermi levels using[24]

$$\rho_{sh}=\frac{\partial\mu/\partial x}{I_{DS}/W}. \tag{18}$$

The derived resistivity, at low drain and high gate voltage ($V_{DS}=10$ mV, $V_{GS}=0.4$ V) is plotted in Fig. 6(b). The sheet resistivity can be divided into the following regions: (1) quantum contact resistance, (2) S/D extension resistance, (3) tip resistance, and (4) channel resistance. Note that the gate modulates the channel resistance and a fraction of the tip resistance only. Therefore, in our device (with a channel mobility of 200 $cm^2/V\,s$), the on current is primarily limited by the S/D parasitic resistances (S/D mobility is just 55 $cm^2/V\,s$). Figure 7(a) plots the I_{DS} versus V_{DS} characteristics in the on state ($V_{GS}=V_{DD}=0.4$ V). For a ballistic off current of 10 $\mu A/\mu m$, the simulated on current in the presence of scattering, is only 50% of the ballistic limit due to S/D and tip parasitics. To reinforce this point, we plot the on current as a function of channel mobility in Fig. 7(b). The channel mobility is progressively increased from zero to very high values. It is clear from Fig. 7(b), that the on current saturates at ~55% of the ballistic limit, and does not increase with increasing channel mobility because of the parasitic resistances. It is expected that transistors with a double-gate geometry will yield twice the on current when compared against those with a single gate (SG) geometry for the same level of off current. This expectation will definitely be met in the ballistic limit. However, if series resistance limits device performance, the performance of a DG MOSFET is degraded to a greater extent than a transistor with a SG geometry. Therefore, the performance benefit expected from DG tran-

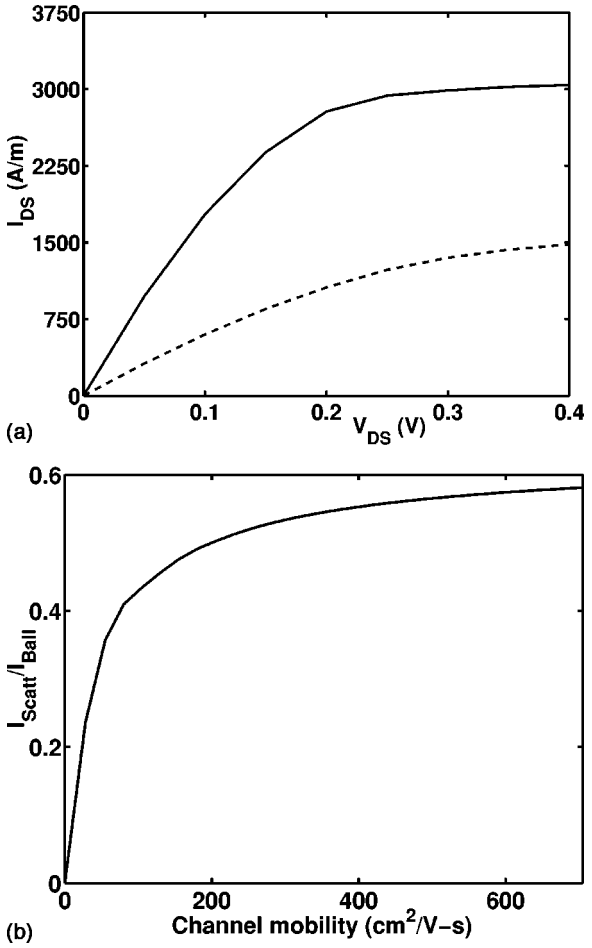

FIG. 7. (a) I_{DS} vs V_{DS} characteristics from the ballistic (solid line) and energy relaxed scattering models (dashed line) for $V_{GS}=0.4$ V. The on-current in the presence of scattering is ~50% of the ballistic limit. (b) The on current vs channel mobility is plotted to indicate that the ultimate performance of our device is primarily controlled by device parasitics.

sistors may not be met. Our model enables us compare DG and SG MOSFETs from the ballistic to the diffusive limit and serves as a valuable design tool to evaluate device design and performance. It captures the essential physics of ballistic and dissipative transport in nanoscale, SOI transistors.

IV. DISCUSSION

In this section we assess the behavior of the energy and phase relaxing scattering models in order to ascertain their applicability to modeling electron transport within a MOSFET. To understand the physics of scattering that is captured by each model, we compare their performance to an analytic theory presented in Ref. 23, where the essential physics of scattering is outlined. We choose to compare the energy and phase relaxing scattering models nonself consistently, in order to avoid the complicated behavior associated with self-consistent electrostatics.[25] Self consistency is important, and we discuss it briefly at the end of this section. Scattering can occur anywhere inside the device, but as shown in Ref. 23, those scattering events that occur in the low field region near the source have the largest effect on the

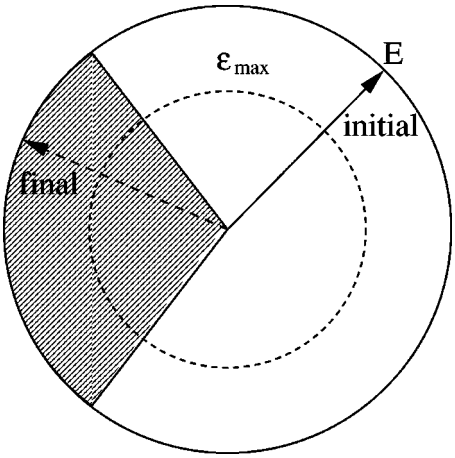

FIG. 8. A pictorial representation of the essential physics of scattering (also refer Fig. 2). The fraction of the scattered electrons that can surmount the source-to-channel barrier and make it back into the source, reduces as we move towards the drain. These carriers, whose total energy is E, are delineated by the cone.

on current. To understand why the importance of backscattering reduces from the source to the drain, we consider a single electron injected from the source into the channel with a total energy, E (note that E_L is its longitudinal energy). Figure 8, tracks this electron in 2D momentum space (initial state is the solid arrow in Fig. 8). Now assume that this electron undergoes a single elastic, isotropic scattering event in the channel (final state is the dotted arrow in Fig. 8). For this electron to make it ballistically back to the source, its longitudinal energy should be greater than ϵ_{max} (Fig. 2). It is clear from Fig. 8 that only a small cone of electrons have enough longitudinal energy to backscatter into the source and that this cone reduces as we move towards the drain (ϵ_{max} increases, and the dotted circle approaches the solid circle in Fig. 8). Therefore, scattering near the source affects the current more strongly than near the drain.

Figure 9 shows the effect of scatterer placement on the device performance from both, the energy and phase relaxing

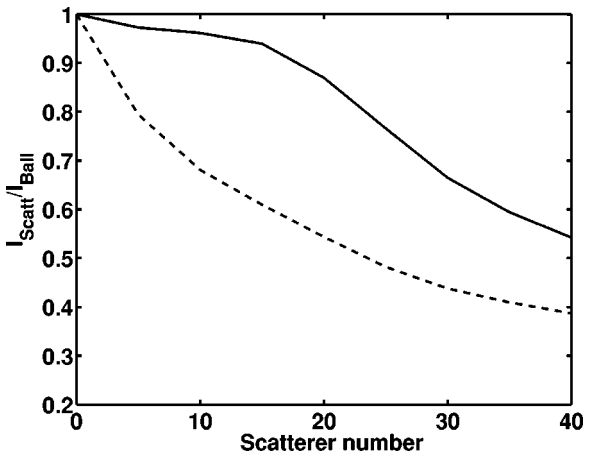

FIG. 9. The current as a function of the scatterer number (placed only in the channel region), which is progressively increased from the drain to the source is plotted from both, the energy relaxing (solid line) and the phase relaxing scattering models. This plot indicates that the energy relaxed model captures the essential physics of scattering in transistors.

models. This figure is generated by fixing the potential profile (ballistic on state) and increasing the number of scatterers progressively from the drain towards the source. When the scatterer number is zero, both models yield the ballistic limit. But as the scatterer number is increased, the energy relaxing scattering model shows very little change in current initially and a linear drop thereafter. When scatterers are placed near the end of the channel, and scattering treated using the energy relaxing model, electrons scatter near the drain and lose much of their longitudinal energies. This makes it difficult for a backscattered electron to make it back to the source. Therefore, the current is initially unaffected. However, as the number of scatterers increases towards the source, electrons scattering very near the source-to-channel barrier do backscatter back into the source as they have not dissipated enough longitudinal energy, thus reducing the current. The phase breaking model shows distinctly different results. The transmitted current decreases with increasing number of scatterers irrespective of their location. This is because, in this model, electrons can reverse direction without losing their channel directed energy. Therefore, scattering anywhere in the channel can reflect electrons back into the source. It should be noted that our qualitative argument considered the effect of elastic scattering alone, and that the addition of any other scattering mechanism serves to relax the longitudinal energy even more. This further reduces the probability (non-self-consistently) of an electron backscattering all the way to the source from the drain end of the device. Therefore, an assessment of the two models clearly indicates that the energy relaxing scattering model, which captures the essential physics of scattering, is the better model to simulate dissipative transport in nanoscale transistors.

Having selected the energy relaxing scattering model, we use it to examine the importance of scattering near the source and drain ends of the device including self-consistent effects. We divide the device into two halves and consider two cases; In the first case, scattering (mobility of 100 $cm^2/V\,s$) is turned on in the first half of the device while the second half is ballistic, and in the second case scattering is turned on in the second half of the device while the first half is ballistic. Our self-consistent simulation results using the energy relaxing model indicate that irrespective of the region where scattering is turned on, the on current is significantly degraded ($\sim$43% in the first case and $\sim$33% in the second case) when compared to the ballistic limit. To understand this behavior, we plot the self-consistent subband profile and 2D charge density for both cases in Fig. 10. When scattering is introduced only in the first half of the device, the on current is strongly degraded when compared to the ballistic limit due to backscattering of electrons at and around the top of the source-to-channel barrier (Fig. 10). Scattered electrons can easily re-enter the source region as they still preserve most of their channel directed energy and hence reduce the net current. When scattering is turned on in the second half of the device alone, the reduction in on current is due to a complicated interplay between self consistency and the effect of scattering.[25] The ballistic stream of source injected electrons entering the second half of the device undergoes scattering.

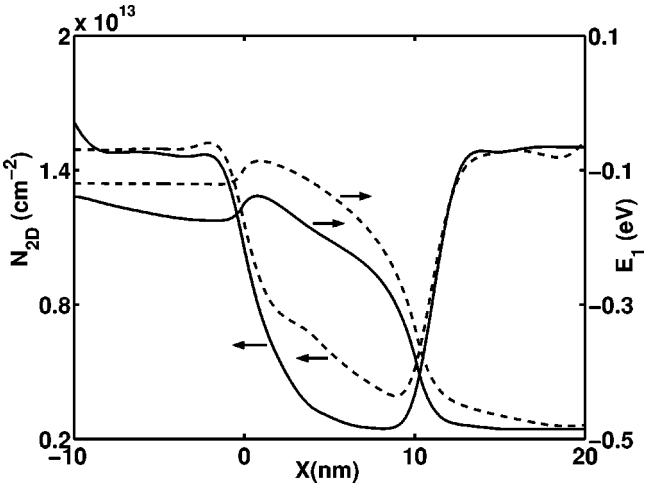

FIG. 10. The profile of the first mode and the 2D electron density in the on state with scattering turned on in the first half of the device (solid lines) and with scattering turned on in the second half of the device (dashed lines). Note that the potential drops in the source or the drain only when scattering is turned on. Also note that turning on scattering only in the second half of the device increases the 2D electron density in the channel.

Once reflected, if the mean free path of these electrons is comparable to the channel length (mean free path is $\sim$10 nm for a mobility of 100 $cm^2/V\,s$) a fraction of these scattered electrons makes it back to the source. This is the first mechanism that reduces the on current. The second mechanism is because the electrons reflected in the second half of the device result in an increased 2D electron density in the channel as shown in Fig. 10 (dotted line). Self consistency causes the subband potential to float to higher energies in the channel and also broadens the potential profile from the source to the drain. An increased source-to-channel barrier combined with a broadened potential profile (which increases the probability of a backscattered electron to re-enter the source as seen from Fig. 8) causes the on current to decrease further when scattering is turned on the second half of the device. This self-consistent behavior of the on current as a function of scatterer placement clearly indicates that scattering is important not only at the source but throughout the channel in nanoscale transistors. This behavior of the on current, when the channel length is comparable to or shorter than the mean free path, has also been observed when scattering is treated rigorously using the Green's function formalism by Ref. 25. The energy relaxed, Büttiker probe based scattering model thus captures all the essential physics of scattering within a MOSFET, including self-consistent effects in a simple and elegant fashion.

V. SUMMARY

We presented a computationally efficient method to quantum mechanically treat the effects of dissipative transport in thin body, fully depleted, SOI transistors including the effect of degeneracy. The proposed model is single parameter model, and the quantum mechanical parameter was related to a low field mobility using simple analytical expressions. We then applied our model to treat the effects of dissipative transport in an ultrathin body (1.5 nm), DG,

n-MOSFET. In doing so, quantum effects that are observed in nanoscale transistors, the role of scattering, effect of parasitics and the treatment of open boundaries were highlighted and discussed. We also presented and discussed the essential physics of scattering in relation to the energy and phase relaxing scattering models and showed that the energy relaxing model was better suited for modeling electron transport in transistors.

Our scattering model is a one parameter model, and the parameter we use can be analytically related to a low field mobility. Such a relation, enables the use of our model to explore physics and device design issues in nanoscale transistors because it can be calibrated to experimentally measured mobility data. This scattering model is also very useful because the detailed NEGF formalism can be used to motivate changes to the nature of the Büttiker probes to mimic the effects of scattering in different material systems such as carbon nanotubes and molecules by appropriately changing the probe self energy. Our model provides an excellent tradeoff between increased computational cost and the physics of scattering that needs to be captured in devices of the future.

ACKNOWLEDGMENTS

The authors would like to thank the Semiconductor Research Corporation for funding this project. The authors are indebted to Zhibin Ren (IBM) whose PhD thesis laid the foundation for the work presented in this article. Useful discussions with J. Rhew and P. Damle from Purdue University, M. Anantram from NASA, and D. Jovanovic from Motorola are also appreciated. R. Venugopal is supported by an Intel PhD Fellowship.

APPENDIX A: THE SELF-ENERGY CALCULATION FOR THE BÜTTIKER PROBES

To illustrate the self-energy calculation which accounts for the device leads and the Büttiker probes, we consider the effect of coupling the Hamiltonian for mode i [Eq. (4)] to a probe at site m (Fig. 2). It is always possible to number the nodes within the mode (i) and the probe, such that the Hamiltonian for the mode plus the probe can be expressed as

$$h=\begin{bmatrix} h_{i,\text{device}} & U_p \\ U_p^{\dagger} & h_{i,\text{probe}} \end{bmatrix}, \tag{A1}$$

where

$$h_{i,\text{probe}}=\begin{bmatrix} 2t_{x,i}+E_i(m) & -t_{x,i} & 0 & \cdots \\ -t_{x,i} & \ddots & \ddots & \ddots \\ \ddots & \ddots & \ddots & \ddots \end{bmatrix}$$

and

$$U_p=\begin{bmatrix} 0 & \cdots & \cdots \\ 0 & \cdots & \cdots \\ U_p^m & 0 & \cdots \end{bmatrix}. \tag{A2}$$

Note that the Hamiltonian representing the probe at site m has the same form as the Hamiltonian for mode i and that the potential within the probe is assumed to be a constant (fixed by the potential at node m for mode i). Therefore, the diagonal elements of the probe Hamiltonian repeat themselves. The choice of $E_i(m)$ and t_x to be the same in the probe and the device ensures that the DOS spectrum within the probe coincides with that within the device. The reason for this choice is explained in Sec. II. The Green's function can in turn be partitioned as

$$\begin{bmatrix} G_{i,\text{device}} & G_{\text{device,probe}} \\ G_{\text{probe,device}} & G_{i,\text{probe}} \end{bmatrix} = \begin{bmatrix} E_L I-h_{i,\text{device}} & -U_p \\ -U_p^{\dagger} & E_L I-h_{i,\text{probe}} \end{bmatrix}^{-1}. \tag{A3}$$

The matrix block we are interested in is $G_{i,\text{device}}$ as we do not care about the Green's function within the probe. Using Eq. (A3) $G_{i,\text{device}}$ can be expressed in terms of known quantities as[7]

$$G_{i,\text{device}}[E_L]=[E_L I-h_{i,\text{device}}-\Sigma_{i,\text{probe}}[E_L]]^{-1}, \tag{A4}$$

where the probe self-energy matrix is

$$\Sigma_{i,\text{probe}}[E_L]=\begin{bmatrix} 0 & 0 & \cdots \\ 0 & 0 & \cdots \\ -U_{p,i}^m & 0 & \cdots \end{bmatrix} \times \left[\begin{array}{c|ccc} E_L I-(2t_{x,i}+E_i^m) & -t_{x,i} & 0 & \cdots \\ \hline -t_{x,i} & \ddots & \ddots & \ddots \\ 0 & \ddots & \ddots & \ddots \end{array}\right]^{-1} \times \begin{bmatrix} \cdots & 0 & -U_{p,i}^m \\ \cdots & 0 & 0 \\ \cdots & \cdots & \cdots \end{bmatrix}. \tag{A5}$$

Note that for evaluating the matrix product in Eq. (A5), we only need the first element of the inverse of the infinite matrix associated with the probe. Also, note that the diagonal blocks of this infinite matrix are repeated due to invariance of the potential within the probe [Eq. (A2)]. Using this property, and partitioning the matrix as shown in Eq. (A5), a closed form expression for the first element of the inverse (denoted by $g_{i,\text{probe}}$) of the infinite matrix can be obtained as

$$I=g_{i,\text{probe}}[E_L I-(2t_{x,i}+E_i^m)-U_p^m g_{i,\text{probe}} U_p^m]. \tag{A6}$$

Once $g_{i,\text{probe}}$ has been solved for, we have

$$\Sigma_{i,\text{probe}}=\begin{bmatrix} 0 & \cdots & 0 \\ 0 & \cdots & 0 \\ 0 & \cdots & U_{p,i}^m g_{i,\text{probe}} U_{p,i}^m \end{bmatrix}. \tag{A7}$$

Note that only node m of the device couples to the probe. Therefore the self energy for the probe [Eq. (A7)] has a single nonzero entry that perturbs the (m,m)th diagonal entry of the mode-space Hamiltonian. By replacing U_p^m, with $t_{x,i}$ in Eq. (A7) we can easily obtain the self-energy for the S/D leads in a similar manner.

APPENDIX B: THE RELATION BETWEEN THE BÜTTIKER PROBE SELF ENERGY AND THE LOW FIELD MOBILITY

In order to relate the probe self energy to a mobility, we first relate it to a mean free path, λ_i. To do so, consider a single mode (we drop the subscript *i* for convenience) with a uniform potential, which is coupled to S/D contacts and N identical Büttiker probes, each of which has the same coupling strength, U_p. The spacing between adjacent probes is a. If a unit amplitude is injected from the source (left contact), the net transmission [denoted $T(N)$] from the source to the drain can be expressed as

$$\frac{1-T(N)}{T(N)} = N\frac{1-T_p}{T_p}, \tag{B1}$$

where T_p is the net transmission across a single probe. Note that Eq. (B1) has been derived by invoking the additive property of $(1-T_p)/T_p$.[9] The net transmission across a single probe, in terms of the transmission into the probe (denoted by T_p^{in}) is

$$T_p = 1 - \frac{T_p^{\text{in}}}{2}. \tag{B2}$$

The reason T_p does not equal T_p^{in}, is because each probe isotropically reinjects electrons into the system in order to conserve charge. Substituting Eq. (B2) into Eq. (B1) and solving for $1/T(N)$ we obtain

$$\frac{1}{T(N)} = 1 + N\frac{T_p^{\text{in}}/2}{1-T_p^{\text{in}}/2} = 1 + \frac{L}{a}\frac{T_p^{\text{in}}/2}{1-T_p^{\text{in}}/2} \sim 1 + \frac{L}{\lambda}, \tag{B3}$$

where L is the distance from the source to the drain. The transmission into a single probe is obtained analytically using Eq. (10). In the weak scattering limit ($U_p \sim 0$, therefore $T_p^{\text{in}} \sim 0$), the final form of the mean free path [from Eq. (B3)] in terms of the lattice spacing a is

$$\lambda = 2a\frac{t_x^2}{U_p^2}$$

where

$$T_p^{\text{in}} = \frac{U_p^2}{t_x^2}. \tag{B4}$$

Once the mean free path is obtained, it can be related to the diffusion coefficient through Schokley's relation, which in turn is related to the low field mobility through Einstien's relation.[23] The relation between the low field mobility and the mean free path is

$$\text{mobility} = \lambda\sqrt{\frac{q^2}{2\pi k_B T m_x^*}} \times \frac{F_{-1/2}(\mu - E_{\text{mode}})F_{-1}(\mu - E_{\text{mode}})}{F_0^2(\mu - E_{\text{mode}})}, \tag{B5}$$

where the arguments to the Fermi functions have been normalized by k_BT and E_{mode} represents the potential energy of electrons in a specific mode. Equations (B4) and (B5) relate the low field mobility to the Büttiker probe strength. Note that the degeneracy factors in Eq. (B5) are position dependent because the mode energy is position dependent. Also note that in our analysis, we assumed single mode occupancy. If several modes are occupied, the mean free path can be interpreted as an average mean free path for all modes and the equivalent mobility as an average low-field mobility for all electrons. The Büttiker probe strength in this case is adjusted differently for each mode (because t_x is mode dependent) to reflect the same average mean free path for all modes.

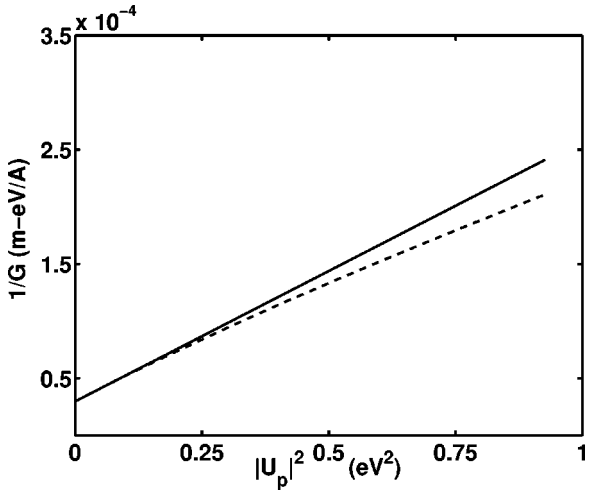

FIG. 11. The low bias conductance for a 40 nm resistor is plotted as a function of scattering strength, from analytical (solid line) expressions and self-consistent simulations (dashed line). The analytic conductance matches the simulated value to within ~10%, indicating that our relation between the Büttiker probe strength and the mean free path [Eq. (B4)] is physically correct.

In order to verify the validity of our derivation, we simulate a uniformly doped resistor (thickness=1.5 nm, length=40 nm, $N=161$, and doping=$10^{20}/\text{cm}^3$) self consistently in the linear response region (low V_{DS}) for different probe strengths [or alternatively, mean free paths evaluated using Eq. (B4)]. The low bias conductance extracted from numerical simulations is compared against analytical values obtained using Eq. (B3) in Fig. 11. [Note that the conductance is directly proportional to $T(N)$.][9] Based on our analytical expressions [Eqs. (B3) and (B4)], we expect a linear relationship between the inverse of the conductance and the inverse of the mean free path. It is clear from Fig. 11 that the numerical and analytical values are in close agreement (within 10%) over a wide range of scattering strengths ranging from a mean free path of ∞ (pure ballistic transport), down to 5 nm. This plot clearly validates our interpretation of the Büttiker probe strength and enables us calibrate quantum mechanical parameters to experimental mobility data in a simple and elegant fashion. The slight discrepancy between the numerical and analytical values is because our analytical expressions are derived in the weak scattering limit.

[1] www.intel.co/labs (2001).
[2] http://www.amd.com/us-en/ (2002).
[3] Y. Naveh and K. Likharev, IEEE Electron Device Lett. **21**, 242 (2000).
[4] P. Solomon and S. Laux, Tech. Dig. - Int. Electron Devices Meet., 95 (2001).

[5] J. Knoch, B. Lengeler, and J. Appenzeller, IEEE Trans. Electron Devices **49**, 1212 (2002).
[6] S. Datta, J. Phys.: Condens. Matter **2**, 8023 (1990).
[7] S. Datta, Superlattices Microstruct. **28**, 253 (2000).
[8] M. Buttiker, Phys. Rev. Lett. **57**, 1761 (1986).
[9] S. Datta, *Electronic Transport in Mesoscopic Systems* (Cambridge University Press, Cambridge, U.K., 1997).
[10] M. Ancona, Superlattices Microstruct. **7**, 119 (1990).
[11] D. Ferry, Superlattices Microstruct. **27**, 61 (2000).
[12] M. Lundstrom, IEEE Electron Device Lett. **18**, 361 (1997).
[13] R. Venugopal, Z. Ren, S. Datta, M. Lundstrom, and D. Jovanovic, J. Appl. Phys. (to be published).
[14] J. Guo, S. Datta, and M. Lundstrom, Appl. Phys. Lett. **80**, 3192 (2002).
[15] C. Texier and M. Buttiker, Phys. Rev. B **62**, 7454 (2000).
[16] P. V. Halen and D. Pulfrey, J. Appl. Phys. **57**, 5271 (1985).
[17] M. de Jong and C. Beenakker, Physica A **230**, 219 (1996).
[18] www.itrs.net (2001).
[19] M. Ieong *et al.*, Tech. Dig. - Int. Electron Devices Meet., 441 (2001).
[20] D. Esseni, M. Mastrapasqua, C. Fiegna, G. Celler, L. Selmi, and E. Sangiorgi, Tech. Dig. - Int. Electron Devices Meet., 445 (2001).
[21] K. Uchida, J. Koga, R. Ohba, T. Numata, and S. Takagi, Tech. Dig. - Int. Electron Devices Meet., 633 (2001).
[22] S. Takagi, J. Koga, and A. Toriumi, Tech. Dig. - Int. Electron Devices Meet., 219 (1997).
[23] M. Lundstrom and Z. Ren, IEEE Trans. Electron Devices **49**, 133 (2001).
[24] Y. Taur and T. Ning, *Fundamentals of VLSI Devices* (Cambridge University Press, Cambridge, U.K., 1998).
[25] A. Svizhenko and M. Anantram (unpublished).

A simple quantum mechanical treatment of scattering in nanoscale transistors

R. Venugopal, M. Paulsson, S. Goasguen, S. Datta, and M. S. Lundstrom

Citation: **93**, (2003); doi: 10.1063/1.1563298
View online: http://dx.doi.org/10.1063/1.1563298
View Table of Contents: http://aip.scitation.org/toc/jap/93/9
Published by the American Institute of Physics